Spatial patterning of endothelial cells and vascular network formation using ultrasound standing wave fields

Kelley A. Garvin and Diane Dalecki
Department of Biomedical Engineering, University of Rochester, Rochester, New York 14627

Mohammed Yousefhussien and Maria Helguera
Chester F. Carlson Center for Imaging Science, Rochester Institute of Technology, Rochester, New York 14623

Denise C. Hocking[a)]
Department of Pharmacology and Physiology, University of Rochester, Rochester, New York 14642

(Received 27 September 2012; revised 15 January 2013; accepted 16 January 2013)

The spatial organization of cells is essential for proper tissue assembly and organ function. Thus, successful engineering of complex tissues and organs requires methods to control cell organization in three dimensions. In particular, technologies that facilitate endothelial cell alignment and vascular network formation in three-dimensional tissue constructs would provide a means to supply essential oxygen and nutrients to newly forming tissue. Acoustic radiation forces associated with ultrasound standing wave fields can rapidly and non-invasively organize cells into distinct multicellular planar bands within three-dimensional collagen gels. Results presented herein demonstrate that the spatial pattern of endothelial cells within three-dimensional collagen gels can be controlled by design of acoustic parameters of the sound field. Different ultrasound standing wave field exposure parameters were used to organize endothelial cells into either loosely aggregated or densely packed planar bands. The rate of vessel formation and the morphology of the resulting endothelial cell networks were affected by the initial density of the ultrasound-induced planar bands of cells. Ultrasound standing wave fields provide a rapid, non-invasive approach to pattern cells in three-dimensions and direct vascular network formation and morphology within engineered tissue constructs. © *2013 Acoustical Society of America*. [http://dx.doi.org/10.1121/1.4812867]

PACS number(s): 43.80.Gx, 43.35.Wa, 43.80.Sh [CCC] Pages: 1483–1490

I. INTRODUCTION

Since the emergence of tissue engineering as a new approach to provide replacement tissue for diseased or injured organs, research and development have led to the clinical implementation of several engineered products (Olson *et al.*, 2011). The first commercially available tissues included skin substitutes and cartilage replacements (Chung and Burdick, 2008; Priya *et al.*, 2008; Jaklenec *et al.*, 2012). More recently, bladder analogs (Atala *et al.*, 2006) and urethral segments (Atala *et al.*, 1999; El-Kassaby *et al.*, 2003; Raya-Rivera *et al.*, 2011) have been successfully implanted into patients, and artificial blood vessels (Shin'oka *et al.*, 2001; L'Heureux *et al.*, 2007; McAllister *et al.*, 2009; Olausson *et al.*, 2012), trachea (Macchiarini *et al.*, 2008; Baiguera *et al.*, 2010), and corneal tissue (Griffith *et al.*, 2009) have reached clinical trials. In contrast, attempts to fabricate larger functional organs that have more complex cellular organization, such as liver, heart, and kidney, have been unsuccessful (Badylak *et al.*, 2012).

The spatial organization of cells in the body is intrinsic to tissue assembly and function. From cardiac and skeletal muscle to blood vessels and ligaments, cellular organization and alignment dictate the mechanical and biological properties of tissues. Alignment of cardiomyocytes is essential for efficient electrical coupling and force transmission in the heart (Pijnappels *et al.*, 2008). In the circulatory system, highly conserved, organ-specific vascular patterns produce a functional circuit (Larrivee *et al.*, 2009). A variety of cell types, including cardiomyocytes and endothelial cells, are responsive to spatial cues and will spontaneously self-organize and align under appropriate conditions (Aubin *et al.*, 2010). Numerous two-dimensional micropatterning techniques have been developed to provide chemical or topographical cues to cells in order to induce cell alignment and trigger self-assembly *in vitro* (Thery, 2010). However, controlling cell alignment in three dimensions to induce tissue formation remains an important challenge in tissue engineering. In particular, developing new techniques to facilitate the generation of functional vasculature would provide a means to supply essential oxygen and nutrients to newly forming tissues and would allow for the creation of more complex organs (Griffith *et al.*, 2005; Khademhosseini *et al.*, 2009).

Endothelial tube formation can be induced *in vitro* when clusters of multiple endothelial cells are arranged a specific distance apart (Korff and Augustin, 1999; Ino *et al.*, 2009) or when cells are encapsulated in collagen gels within microfabricated channels of defined dimensions (Raghavan *et al.*, 2010; Zheng *et al.*, 2012). The diameter of endothelial tubes was shown to increase linearly with increasing microchannel

[a)]Author to whom correspondence should be addressed. Electronic mail: denise_hocking@urmc.rochester.edu

diameter (Raghavan *et al.*, 2010), suggesting that spatial cues can also be utilized to shape vessel morphology. In previous studies, we demonstrated that acoustic radiation forces associated with ultrasound standing wave fields can rapidly and non-invasively organize cells spatially into distinct multicellular planar bands within three-dimensional (3D) collagen gels (Garvin *et al.*, 2010). Ultrasound standing wave field-induced alignment of endothelial cells led to the formation of lumen containing, branching vessel networks throughout the complete volume of the collagen construct (Garvin *et al.*, 2011). Here, we investigated the effects of various ultrasound standing wave field exposure parameters on the initial spatial pattern of endothelial cells within collagen hydrogels, and the morphology of the resultant vascular networks. Our studies demonstrate that spatial patterning of endothelial cells within 3D collagen gels can be controlled by design of frequency and temporal average intensity of the sound field. In turn, ultrasound-induced spatial patterning of endothelial cells directly affects the morphology of the resultant vascular network.

II. MATERIALS AND METHODS

A. Ultrasound standing wave field exposure apparatus

The experimental setup used for ultrasound standing wave field exposures has been described previously (Garvin *et al.*, 2010; Garvin *et al.*, 2011). A plastic exposure tank was filled with degassed, deionized water. The acoustic source, either a 1-MHz unfocused (2.5 cm diameter) or a 2-MHz unfocused (1.25 cm diameter) piezoceramic transducer, was placed at the bottom of the exposure tank. A waveform generator (Hewlett Packard, Model 33120A, Palo Alto, CA), an attenuator (Kay Elemetrics, model 837, Lincoln Park, NJ), and a radio-frequency power amplifier (ENI, Model 2100L, Rochester, NY) were used to generate the ultrasound signal driving the transducer. Samples were contained within acoustically transparent, silicone elastomer-bottomed cell culture plates (FlexCell International Corporation, BioFlex® plates, Hillsborough, NC) that had been modified to reduce the well diameter to 1 cm using elastomer molds (Sylgard® 184 silicone elastomer; Dow Corning Corporation, Midland, MI) (Garvin *et al.*, 2010). Previous work (Garvin *et al.*, 2010) characterized the attenuation of the sample holder and measured the standing wave fields generated within the sample holder volume. Sample holders were connected to a three-axis positioner (Velmex, Series B4000 Unislide, East Bloomfield, NY) to accurately control the sample location within the sound field. Plate bottoms were situated near the air–water interface in the far-field of each transducer, at an axial distance of 12.2 cm for the 1-MHz source or 13 cm for the 2-MHz transducer. The reflection from the air interface above the sample resulted in the production of an ultrasound standing wave field within the sample volume (Garvin *et al.*, 2010; Garvin *et al.*, 2011).

Prior to each experiment, a needle hydrophone (Onda Corporation, HNC-0400, Sunnyvale, CA) was used to calibrate the acoustic field under traveling wave field conditions. Acoustic pressure measurements were made at axial distances of 12.2 cm from the 1-MHz transducer and 13 cm from the 2-MHz source, where sample holders were placed for standing wave field exposures. The transaxial −6 dB beam widths of the 1- and 2-MHz transducers were 1.2 cm at the above stated axial locations. To locate samples within the acoustic field, coordinates obtained from the hydrophone calibration were used to position well bottoms of the cell culture plates at the air–water interface for the above stated axial locations from each transducer (12.2 cm for 1-MHz and 13 cm for 2-MHz). Ultrasound standing wave field-exposed samples were positioned such that the maximum acoustic pressure in the transaxial direction was centered within the well at the desired axial locations listed above.

B. Cell culture

Human umbilical vein endothelial cells (Vec Technologies, Rensselear, NY; pooled donor) were routinely cultured in MCDB-131 growth medium (Invitrogen, Carlsbad, CA) supplemented with 10% fetal bovine serum (HyClone, Logan, UT), L-glutamine (Invitrogen, Carlsbad, CA), and ENDO GRO® growth factor (Vec Technologies, Rensselear, NY). Endothelial cells were harvested using 0.05% trypsin/EDTA (Invitrogen, Carlsbad, CA) and resuspended in MCDB-131 growth medium. All experiments were performed using cells between passage 3 and 8.

C. Cell-embedded collagen gels

Neutralized type I collagen solutions were prepared on ice by mixing type I collagen (BD Biosciences, Bedford, MA; from a rat tail) with 2× concentrated Dulbecco's modified Eagle's medium (DMEM; Invitrogen, Carlsbad, CA) and 1× DMEM such that the final mixture contained 1× DMEM and 0.8 mg/ml collagen (Garvin *et al.*, 2010; Garvin *et al.*, 2011). The 1× and 2× DMEM were degassed for 30 min in a vacuum chamber under sterile conditions prior to incorporation into the collagen mixture. Endothelial cells were added to aliquots of the collagen solution at final concentrations of either 1×10^6 cell/ml or 4×10^6 cell/ml immediately prior to ultrasound standing wave field exposure.

D. Ultrasound standing wave field exposures

For each exposure, aliquots of unpolymerized solutions of collagen and endothelial cells were added to two wells of the sample holder. One sample was exposed to an ultrasound standing wave field at either 1 or 2 MHz for 15 min in a room temperature water tank. The other sample was treated exactly as the ultrasound-exposed sample but was not subjected to ultrasound standing wave field exposure and thus served as the sham exposure condition. For experiments at 1 MHz, samples were exposed to either continuous wave (CW) or pulsed ultrasound (20 μs pulse duration, duty cycles of 0.12, 0.24, or 0.5) at various peak positive acoustic pressures (0 to 0.3 MPa) and spatial peak temporal average intensities ($I_{spta} = 0$ to 2.4 W/cm^2). Acoustic pressures reported are the maximum peak positive pressure at an antinode, and reported intensities are the spatial peak temporal average intensity (I_{spta}) calculated at an antinode. For experiments at

2 MHz, samples were exposed to CW ultrasound at peak positive acoustic pressures of 0 to 0.2 MPa (I_{spta} of 0 to 1.6 W/cm^2). The 15 min exposure duration was sufficient to allow for collagen polymerization within the room temperature water tank.

Following ultrasound standing wave field exposure, cell-embedded collagen gels were incubated for either 20 min (for experiments investigating initial cell band formation) or 1 h (for experiments investigating endothelial cell network formation) at 37 °C and 5% CO_2. An equal volume of MCDB-131 growth medium supplemented with 20 ng/ml phorbol myristate acetate (Sigma, St. Louis, MO) was then added to each collagen gel (Garvin *et al.*, 2011). Samples designated for analysis of initial cell band formation were visualized using phase-contrast microscopy. Samples designated for analysis of endothelial network formation were maintained at 37 °C and 5% CO_2, and the medium was changed daily.

E. Microscopy and immunostaining

Endothelial cell bands and vessel networks within ultrasound standing wave field- and sham-exposed samples were examined at various times using phase-contrast or multiphoton immunofluorescence microscopy. Studies were performed on three separate experimental days with at least duplicate samples for each exposure condition in each experiment. Phase-contrast microscopy was performed using an inverted microscope (Carl Zeiss MicroImaging, Thornwood, NY) equipped with a 5× or 10× phase-contrast objective, and samples were photographed using a digital camera (Model Infinity 2; Lumenera, Ottawa, ON, Canada). Viable endothelial cells were visualized on Days 4 and 10 after ultrasound exposure by staining with thiazolyl blue tetrazolium bromide (MTT) (Garvin *et al.*, 2011).

Multiphoton immunofluorescence microscopy was used to visualize endothelial cell networks within the 3D collagen gels. Briefly, ultrasound- and sham-exposed collagen gels were cultured for 10 days, then fixed and permeabilized, as described previously (Garvin *et al.*, 2011). Endothelial cells were visualized by immunostaining for CD31 using a mouse anti-human CD31 monoclonal antibody (clone MEM-05; Invitrogen, Carlsbad, CA) followed by an Alexa Fluor® 594-conjugated goat anti-mouse IgG secondary antibody (Invitrogen, Carlsbad, CA). Cell nuclei were labeled with 60 nM 4′,6-diamidino-2-phenylindole (DAPI) dilactate (Invitrogen, Carlsbad, CA). Collagen gel samples were examined using an Olympus Fluoview 1000 AOM-MPM microscope equipped with a 25×, 1.05 NA water immersion lens (Olympus, Center Valley, PA). Samples were illuminated with 780 nm light generated by a Mai Tai HP Deep See Ti:Sa laser (Spectra-Physics, Mountain View, CA) and the emitted light was detected with a photomultiplier tube using two bandpass filters, one with a 460 nm center wavelength (Filter FF01-460-80; Semrock, Rochester, NY) to visualize DAPI staining and the second with a 609 nm center wavelength (Filter FF01-609/54-25; Semrock, Rochester, NY) to visualize CD31 staining simultaneously. Images were collected using a CMOS digital camera (Moticam 1000; Motic, Xiamen, China).

Quantitative texture feature analysis was performed on multiphoton images of endothelial vessel networks (Day 10) formed in response to different ultrasound exposure parameters. *Z*-stack images, each containing ~300 sections acquired at step intervals of 1 μm, were pre-processed to rescale intensity, 3D median filter, and equalize contrast using contrast limited adaptive histogram equalization (Pang *et al.*, 2009). A 3D connected component analysis was performed on the preprocessed image stacks (Pang *et al.*, 2009). The textural features, contrast and entropy, were extracted from the Gray Level Co-occurrence Matrix of the preprocessed image (Haralick, 1979). Contrast is commonly defined as a measure of the difference between the brightest and darkest intensity values of contiguous pixels (Gonzalez and Woods, 2008). Entropy measures randomness in the sample (Gonzalez and Woods, 2008).

III. RESULTS

A. Spatial patterning of cells with ultrasound standing wave fields

Collagen gels embedded with endothelial cells were fabricated using 1 and 2 MHz ultrasound standing wave fields. Representative phase-contrast microscopy images of resultant gels are shown in Fig. 1. Samples not exposed to ultrasound were characterized by a homogeneous distribution of cells ["Sham," Figs. 1(A) and 1(B)]. In contrast, exposure of samples to ultrasound standing wave fields of appropriate pressure amplitudes prior to collagen gel polymerization resulted in the directed movement of cells toward the pressure nodes (Fig. 1). The exposure geometry used for these studies produced an ultrasound standing wave field throughout the exposure volume that was characterized by planar nodes spaced at one-half wavelength intervals (Garvin *et al.*, 2010). Thus, the resulting spatial pattern produced by the ultrasound standing wave field consisted of planar bands of endothelial cells that were distributed throughout the collagen gel volume.

For exposures at 1 MHz, planar bands of cells were observed at pressure amplitudes of 0.1 MPa (as measured at an antinode) and above [Fig. 1(A)]. At the exposure amplitude of 0.1 MPa, planar bands contained loosely aggregated cells. This pressure amplitude corresponds to a calculated I_{spta} value of 0.28 W/cm^2. As the pressure amplitude of exposure increased, the density of cells within the planar bands also increased [Fig. 1(A)]. The measured distance between cell bands at the exposure amplitude of 0.3 MPa was 779.5 μm ± 29.7 μm, which agrees well with the calculated one-half wavelength at 1 MHz of 750 μm.

Ultrasound standing wave field-induced planar bands of cells were separated by a distance corresponding to half of the wavelength of sound exposure. As such, choice of the ultrasound standing wave field frequency should allow for control over the spacing between planar cell bands. For exposures at 2 MHz, the presence of planar cell bands was evident at pressure amplitudes of 0.08 MPa (as measured at an antinode) and above [Fig. 1(B)]. At the exposure

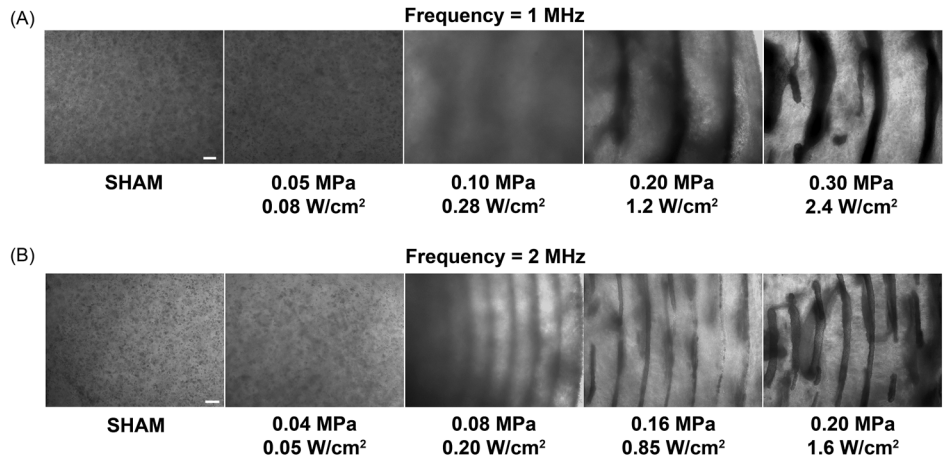

FIG. 1. Spatial patterning of cells within collagen hydrogels using ultrasound standing wave fields. Unpolymerized solutions of type I collagen and endothelial cells (4×10^6 cell/ml) were exposed for 15 min during the polymerization process to either a 1- or 2-MHz CW ultrasound standing wave field. Samples were exposed to various peak positive pressure amplitudes (measured at standing wave field pressure antinodes) and calculated I_{spta} values. Resultant collagen gels were analyzed for cell location using phase-contrast microscopy. Representative side-view images of cell-embedded collagen gels are shown for 1-MHz (A) and 2-MHz (B) experiments ($n = 3$). Scale bar, 200 μm.

amplitude of 0.08 MPa, which corresponds to a calculated I_{spta} value of 0.2 W/cm^2, the planar bands again consisted of loosely aggregated cells. Similar to results obtained at 1 MHz, as the exposure pressure amplitude increased, cell density within the planar bands increased [Fig. 1(B)]. At an exposure amplitude of 0.2 MPa, the measured distance between cell bands was 364.8 μm $\pm$ 15.2 μm, which also agrees well with the calculated one-half wavelength at 2 MHz of 375 μm.

Collectively, these data demonstrate that ultrasound standing wave field exposure parameters can control the spatial pattern of cells within the engineered construct. Choice of acoustic frequency of the standing wave field controls the spacing of the planar bands of cells. For CW exposures of an ultrasound standing wave field, as the pressure amplitude of exposure increased, the resultant spatial pattern of cells within the 3D construct shifted from a homogeneous distribution of cells, to loosely aggregated planar bands of cells, to densely packed cell bands spaced at one-half wavelength intervals.

B. Tests of pressure amplitude and I_{spta}

To develop the use of ultrasound standing wave fields as a technology for non-invasive cell patterning, it is critical to define the acoustic parameters that control ultrasound-induced spatial patterns. In the experiments described above and presented in Fig. 1, CW ultrasound standing wave field exposures were utilized. In those experiments, both the acoustic pressure and the calculated I_{spta} of the sound field were varied. Thus, a series of experiments was conducted next to independently assess the roles of acoustic pressure and I_{spta} in ultrasound-induced spatial patterning of cells.

Figure 2(A) illustrates representative phase-contrast microscopy images of cell-embedded collagen gels fabricated using an ultrasound standing wave field of 1 MHz with a constant antinode pressure amplitude of 0.2 MPa and various I_{spta} values. A constant pressure amplitude of 0.2 MPa was used as this value was above the pressure threshold for ultrasound standing wave field-induced cell banding previously observed for CW exposures (Fig. 1). For these experiments, the ultrasound was pulsed using a 20-μs pulse duration and duty cycles of either 0 (sham), 0.12, 0.24, 0.5, or 1 (CW), corresponding to I_{spta} values of 0, 0.14, 0.28, 0.6, and 1.2 W/cm^2, respectively. As shown in Fig. 2(A), sham-exposed collagen gels, as well as collagen gels exposed to an I_{spta} value of 0.14 W/cm^2, contained homogenously distributed cells. In contrast, at an I_{spta} value of 0.28 W/cm^2, loosely aggregated bands of cells were evident within the 3D gels. Increasing I_{spta} above 0.28 W/cm^2 resulted in the formation of planar bands of cells that were more densely packed [Fig. 2(A)]. These data indicate that the threshold for ultrasound standing wave field-induced cell banding was 0.28 W/cm^2 for a constant pressure amplitude of 0.2 MPa. This agrees with the observed threshold of 0.28 W/cm^2 for CW exposures shown in Fig. 1(A).

Figure 2(B) illustrates representative phase-contrast microscopy images of collagen gels fabricated using an ultrasound standing wave field of 1 MHz with a constant antinode I_{spta} of 0.28 W/cm^2 and various antinode pressure amplitudes. A constant I_{spta} of 0.28 W/cm^2 was utilized, as this value was the threshold for ultrasound standing wave field-induced cell banding observed for both the CW (Fig. 1) and the pulsed [Fig. 2(A)] exposures. For these studies, a pulsed ultrasound field was utilized with a 20-μs pulse duration and duty cycles of either 0 (sham), 0.12, 0.24, 0.5, or 1 (CW), corresponding to antinode pressure amplitudes of 0, 0.30, 0.20, 0.15, and 0.1 MPa, respectively. A homogeneous cell distribution was observed in sham-exposed samples [Fig. 2(B)]. However, at all ultrasound exposure conditions tested, loosely aggregated, planar bands of cells were formed within the engineered construct [Fig. 2(B)]. Collectively, these data demonstrate that the temporal average intensity, not the pressure amplitude, defines the threshold for cell banding, and controls the density of cells within planar bands.

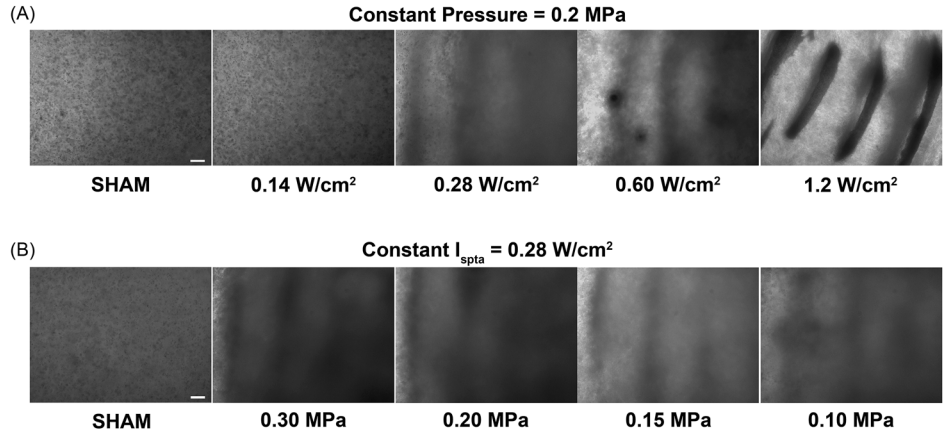

FIG. 2. Dependence of cell patterns on temporal average intensity. Unpolymerized solutions of type I collagen and endothelial cells (4×10^6 cell/ml) were exposed during polymerization to a 1-MHz ultrasound standing wave field. Samples were exposed using (A) a constant ultrasound standing wave field peak positive pressure amplitude (measured at a pressure antinode) of 0.2 MPa and various I_{spta} values, or (B) a constant I_{spta} of 0.28 W/cm^2 and various ultrasound standing wave field peak positive pressure amplitudes. Resultant collagen gels were analyzed for cell location using phase-contrast microscopy. Representative side-view images of cell-embedded collagen gels are shown for both the constant pressure (A) and constant I_{spta} (B) experiments ($n = 3$). Scale bar, 200 μm.

C. Ultrasound-induced spatial patterning of cells controls vascular network morphology

To successfully fabricate complex, 3D tissues *in vitro*, methods that promote vascular network formation within the construct are needed in order to maintain cell viability and tissue function. In our previous work (Garvin *et al.*, 2011), ultrasound standing wave field-mediated organization of endothelial cells into multicellular planar bands within collagen hydrogels led to the rapid and extensive formation of lumen-containing endothelial cell networks throughout the 3D construct. Figures 1 and 2 demonstrate that various spatial patterns of cells can be produced within collagen gels by design of ultrasound standing wave field exposure parameters. The next series of experiments was developed to investigate whether the initial ultrasound standing wave field-induced spatial pattern of cells affects the morphology of the resultant endothelial cell network.

In the first of these experiments, collagen solutions containing endothelial cells were exposed to a CW ultrasound standing wave field at 1 MHz with an I_{spta} of either 0.28 or 2.4 W/cm^2 to produce constructs containing either loosely aggregated or densely packed bands of cells, respectively. Following a 4- or 10-day incubation, endothelial cell networks within the collagen gels were visualized using either MTT staining to identify viable cells (Fig. 3) or multiphoton immunofluorescence microscopy to obtain higher resolution images (Fig. 4). As shown in Fig. 3, collagen gels containing endothelial cells that were initially loosely aggregated within planar bands (0.28 W/cm^2) developed extensive anastomosing networks by Day 4 that were characterized by a tortuous morphology; the morphology of these networks persisted through Day 10 (Fig. 3). In contrast, collagen samples fabricated to initially contain densely packed bands of endothelial cells (2.4 W/cm^2) developed multiple, non-branching, capillary-like sprouts that emerged from the planar cell bands by Day 4 (Fig. 3). By Day 10, these capillary-like sprouts had developed into anastamosing endothelial cell networks (Fig. 3). Sham-exposed collagen samples, in which cells were initially distributed homogeneously, contained elongated cells at the 4-day time point (Fig. 3). By Day 10, any endothelial cell network formation within sham samples was observed only at the bottom of the collagen gel (Fig. 3, inset) and was not found throughout the 3D volume of the sample. These observations indicate that endothelial cell networks developed more rapidly within samples having loosely aggregated cell bands as compared to samples containing either densely packed cell bands or homogeneously distributed cells. Additionally, the morphology of the endothelial cell networks formed within the collagen samples over the 10-day period differed among the three initial ultrasound-induced cell patterns studied in these experiments.

Multiphoton immunofluorescence microscopy was used to further examine the vascular networks formed on Day 10 in response to the different ultrasound standing wave field exposures. Similar to results shown in Fig. 3, collagen gels

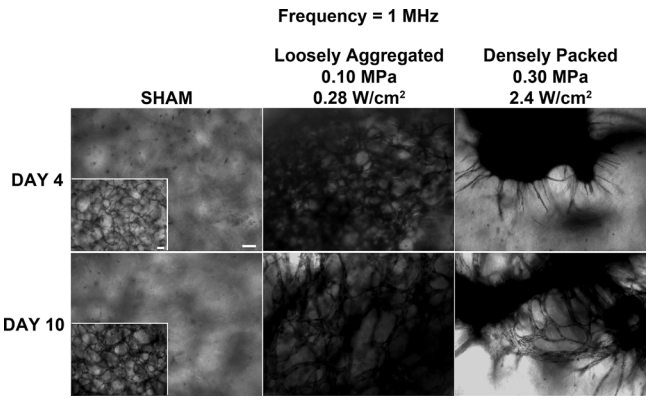

FIG. 3. Morphology of vascular networks produced using ultrasound standing wave fields at 1 MHz. Unpolymerized solutions of type I collagen and endothelial cells (1×10^6 cell/ml) were exposed during polymerization to a 1-MHz CW ultrasound standing wave field. Samples were exposed using antinode pressure amplitudes of 0, 0.1, or 0.3 MPa, which correspond to I_{spta} values of 0, 0.28, and 2.4 W/cm^2, respectively. (A) Resultant collagen gels were incubated at 37 °C for either 4 or 10 days and then analyzed using phase-contrast microscopy and MTT staining. Representative top view images are shown ($n = 3$). Scale bar, 100 μm.

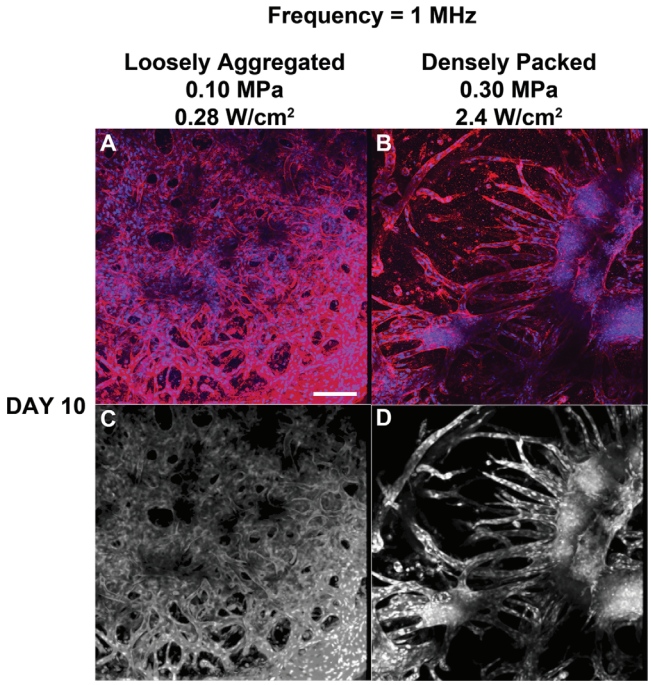

FIG. 4. Analysis of endothelial network morphology formed in response to 1-MHz ultrasound. Unpolymerized solutions of type I collagen and endothelial cells were exposed to a 1-MHz CW ultrasound standing wave field, as described in the legend to Fig. 3. Following a 10-day incubation, samples were processed for immunofluorescence microscopy. CD31 was visualized by staining with a mouse anti-human CD31 monoclonal antibody (red). Cell nuclei were visualized by co-staining with DAPI (blue). Multiphoton microscopy was used to collect top view images along the z axis in 1 μm slices. Images were then projected onto the z-plane using ImageJ software (NIH, Bethesda, MD). Representative z-stack images are shown before [(A) and (B)] and after [(C) and (D)] image processing ($n = 3$). Scale bar, 50 μm.

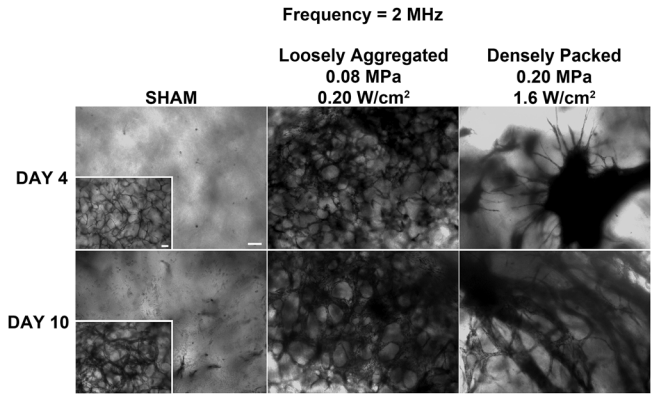

FIG. 5. Morphology of vascular networks produced using ultrasound standing wave fields at 2 MHz. Unpolymerized solutions of type I collagen and endothelial cells (1×10^6 cell/ml) were exposed during polymerization to a 2-MHz CW ultrasound standing wave field. Samples were exposed using antinode pressure amplitudes of 0, 0.08, or 0.2 MPa, corresponding to I_{spta} values of 0, 0.2, and 1.6 W/cm^2, respectively. Resultant collagen gels were incubated at 37 °C for 4 or 10 days and then analyzed using phase-contrast microscopy and MTT staining. Representative top view images are shown ($n = 3$). Scale bar, 100 μm.

fabricated using an ultrasound standing wave field at 1 MHz with an I_{spta} of 0.28 W/cm^2 were characterized by dense, tortuous, anastomosing endothelial cell networks that were evident throughout the 3D volume of the collagen hydrogel [Fig. 4(A)]. Collagen gels fabricated using an I_{spta} of 2.4 W/cm^2 contained vascular networks having tree-like morphologies that originated from planar cell bands [Fig. 4(B)]. Again, any endothelial cell networks formed within sham samples were found only at the base of the collagen construct (not shown).

To quantify the observed differences in endothelial network morphology that developed from either loosely aggregated or densely packed planar cell bands, textural feature analysis was performed on the acquired multiphoton images. Representative images showing the 3D connected component volume are presented in Figs. 4(C) and 4(D). Quantification of textural parameters yielded higher contrast and entropy values for vascular networks formed from loosely aggregated versus densely packed endothelial cell bands (contrast, 20.0 ± 0.5 versus 6.0 ± 2.3; entropy, 3.22 ± 0.21 versus 2.35 ± 0.20 for 0.28 and 2.4 W/cm^2, respectively; $n = 3$). Taken together, these data indicate that both the rate of formation and the morphology of resulting vascular networks were determined by the initial ultrasound-induced spatial density of cells within planar bands.

In the next series of experiments, collagen gels were fabricated using ultrasound standing wave fields at 2 MHz to produce gels with different initial cell band spacing compared to the 1 MHz samples. Collagen/endothelial cell solutions were exposed to a CW ultrasound standing wave field at 2 MHz with I_{spta} of either 0.20 or 1.6 W/cm^2 to produce either loosely aggregated or densely packed planar cell bands, respectively. Following a 4 or 10 day incubation, endothelial cell networks within the collagen samples were visualized using either MTT staining (Fig. 5) or multiphoton immunofluorescence microscopy (Fig. 6). Clear differences in vascular network morphology were again observed depending upon the initial ultrasound-induced spatial patterning of endothelial cells within the collagen construct. Samples initially containing ultrasound-induced planar bands of loosely aggregated cells (0.20 W/cm^2) formed anastomosing endothelial cell networks with a tortuous morphology at Days 4 and 10 (Fig. 5). Samples that were fabricated to contain planar bands of densely packed endothelial cells (1.6 W/cm^2) formed multiple, capillary-like sprouts that emerged from the planar bands by Day 4; by Day 10, these samples contained extensive branching tree-like networks (Fig. 5). Sham-exposed collagen samples contained cells with an elongated morphology at Day 4, and minimal cell networks located only at the bottom of the construct by Day 10 (Fig. 5, inset). Multiphoton immunofluorescence microscopy [Figs. 6(A) and 6(B)] and texture feature analysis of connected component images [Figs. 6(C) and 6(D)] provided further evidence to support the observed differences in vascular network morphologies. Similar to results obtained using 1-MHz ultrasound, quantification of textural parameters yielded higher contrast and entropy values for vascular networks formed from loosely aggregated versus densely packed endothelial cell bands (contrast, 24.4 ± 2.0 versus 9.4 ± 1.2; entropy, 3.27 ± 0.05 versus 2.40 ± 0.19 for 0.20 and 1.6 W/cm^2, respectively; $n = 3$).

IV. DISCUSSION

Acoustic radiation forces associated with ultrasound standing wave fields can spatially organize particles or cells

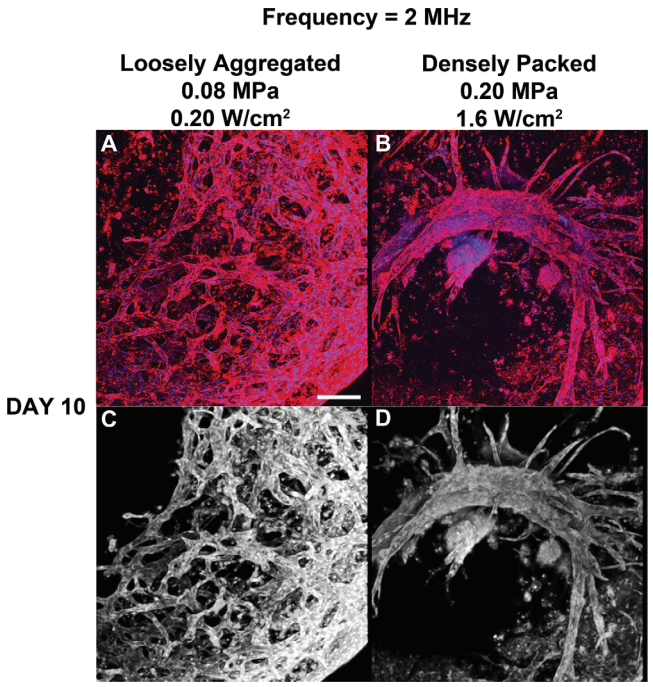

FIG. 6. Analysis of endothelial network morphology formed in response to 2-MHz ultrasound. Unpolymerized solutions of type I collagen and endothelial cells were exposed to a 2-MHz CW ultrasound standing wave field, as described in the legend to Fig. 5. Following a 10-day incubation, samples were processed for immunofluorescence microscopy. CD31 was visualized by staining with a mouse anti-human CD31 monoclonal antibody (red). Cell nuclei were visualized by co-staining with DAPI (blue). Multiphoton microscopy was used to collect top view images along the z axis in 1 μm slices. Images were then projected onto the z-plane using ImageJ (NIH). Representative z-stack images are shown before [(A) and (B)] and after [(C) and (D)] image processing ($n = 3$). Scale bar, 50 μm.

to defined locations in suspending media (Dyson *et al.*, 1974; Whitworth and Coakley, 1992; Coakley *et al.*, 1994; Saito *et al.*, 1998; Bazou *et al.*, 2005; Gherardini *et al.*, 2005; Bazou *et al.*, 2006; Garvin *et al.*, 2011). The primary acoustic radiation force generated along the direction of sound propagation is largely responsible for the movement of cells and particles within an ultrasound standing wave field (Gor'kov, 1962; Gol'dberg, 1971; Gould and Coakley, 1974). In this paper, ultrasound standing wave fields at 1 and 2 MHz were used to fabricate 3D collagen constructs containing spatially patterned endothelial cells. Propagation of ultrasound through the collagen sample and reflection from the media/air interface resulted in the production of an ultrasound standing wave field throughout the sample volume. Standing wave fields were characterized by planes of maximum pressure (antinodes) and planes of zero pressure (nodes) perpendicular to the direction of sound propagation (Garvin *et al.*, 2010; Garvin *et al.*, 2011). Nodal planes were spaced at distances equal to one-half the wavelength of the ultrasound field. Acoustic radiation forces associated with the ultrasound standing wave field resulted in spatial patterning of endothelial cells into planar bands throughout the collagen construct.

Through a series of investigations, we demonstrated that design of acoustic radiation forces associated with ultrasound standing wave fields can be used to noninvasively control the spatial pattern of cells and the morphology of resulting vascular networks within 3D collagen-based constructs. For the geometry investigated here, choice of ultrasound frequency controlled the distance between planar bands of cells. Additionally, the density of cells within each planar band was determined by the temporal average intensity of the sound exposure. Importantly, the initial ultrasound-induced spatial pattern of endothelial cells had significant effects on the resulting vascular network that developed over time in the engineered constructs. Using different ultrasound field exposure parameters, endothelial cells were organized within collagen gels into either loosely aggregated or densely packed planar bands. Both the rate of formation and the morphology of resultant endothelial cell networks were affected by the initial cell density. For the range of parameters investigated herein, the initial spacing between ultrasound standing wave field-induced cell bands (750 μm for 1-MHz ultrasound and 375 μm for 2-MHz ultrasound) did not affect the rate of formation or the morphology of the resultant vascular networks within the hydrogels. Rather, the initial density of the cell bands played a dominant role in defining network morphology.

Technologies capable of controlling the size and morphology of vessels within engineered tissues will allow for the production of tissues with complex vascular network structures. Results of investigations reported in this paper demonstrate that ultrasound standing wave fields provide a non-invasive approach to both pattern cells in three-dimensions within engineered constructs and direct vascular network formation and development. This ultrasound-based approach is advantageous as it does not reduce cell viability, can be adapted to various hydrogels that undergo phase transitions, can be utilized for rapid cell organization throughout large volumes, and can produce vessels with defined lumen sizes and network organizations. Use of multiple transducers and alternate source geometries would allow for the production of other spatial patterns of cells throughout 3D engineered tissues.

V. CONCLUSIONS

Ultrasound standing wave field exposure parameters can control the spatial pattern of cells within collagen hydrogels. Choice of acoustic frequency of the standing wave field controls the spacing of the planar bands of cells. The temporal average intensity defines the threshold for cell banding and controls the density of cells within planar bands. Both the rate of formation and the morphology of resultant vascular networks were determined by the initial density of cells within planar bands. Thus, ultrasound standing wave fields provide a rapid, non-invasive approach to pattern endothelial cells in three-dimensions and direct vascular network formation and morphology within engineered tissue constructs.

ACKNOWLEDGMENTS

This work was supported in part by the National Institutes of Health (Grant No. R01 EB008368). The authors thank Sally Z. Child, Jasmine Carvalho, and Nicholas Berry for technical assistance.

Atala, A., Bauer, S. B., Soker, S., Yoo, J. J., and Retik, A. B. (**2006**). "Tissue-engineered autologous bladders for patients needing cystoplasty," Lancet **367**, 1241–1246.
Atala, A., Guzman, L., and Retik, A. B. (**1999**). "A novel inert collagen matrix for hypospadias repair," J. Urol. **162**, 1148–1151.
Aubin, H., Nichol, J. W., Hutson, C. B., Bae, H., Sieminski, A. L., Cropek, D. M., Akhyari, P., and Khademhosseini, A. (**2010**). "Directed 3D cell alignment and elongation in microengineered hydrogels," Biomaterials **31**, 6941–6951.
Badylak, S. F., Weiss, D. J., Caplan, A., and Macchiarini, P. (**2012**). "Engineered whole organs and complex tissues," Lancet **379**, 943–952.
Baiguera, S., Birchall, M. A., and Macchiarini, P. (**2010**). "Tissue-engineered tracheal transplantation," Transplantation **89**, 485–491.
Bazou, D., Dowthwaite, G. P., Khan, I. M., Archer, C. W., Ralphs, J. R., and Coakley, W. T. (**2006**). "Gap junctional intercellular communication and cytoskeletal organization in chondrocytes in suspension in an ultrasound trap," Mol. Membr Biol. **23**, 195–205.
Bazou, D., Kuznetsova, L. A., and Coakley, W. T. (**2005**). "Physical environment of 2-D animal cell aggregates formed in a short path length ultrasound standing wave trap," Ultrasound Med. Biol. **31**, 423–430.
Chung, C., and Burdick, J. A. (**2008**). "Engineering cartilage tissue," Adv. Drug Delivery Rev. **60**, 243–262.
Coakley, W. T., Whitworth, G., Grundy, M. A., Gould, R. K., and Allman, R. (**1994**). "Ultrasonic manipulation of particles and cells. Ultrasonic separation of cells," Bioseparation **4**, 73–83.
Dyson, M., Pond, J. B., Woodward, B., and Broadbent, J. (**1974**). "The production of blood cell stasis and endothelial damage in the blood vessels of chick embryos treated with ultrasound in a stationary wave field," Ultrasound Med. Biol. **1**, 133–148.
El-Kassaby, A. W., Retik, A. B., Yoo, J. J., and Atala, A. (**2003**). "Urethral stricture repair with an off-the-shelf collagen matrix," J. Urol. **169**, 170–173; discussion 173.
Garvin, K. A., Dalecki, D., and Hocking, D. C. (**2011**). "Vascularization of three-dimensional collagen hydrogels using ultrasound standing wave fields," Ultrasound Med. Biol. **37**, 1853–1864.
Garvin, K. A., Hocking, D. C., and Dalecki, D. (**2010**). "Controlling the spatial organization of cells and extracellular matrix proteins in engineered tissues using ultrasound standing wave fields," Ultrasound Med. Biol. **36**, 1919–1932.
Gherardini, L., Cousins, C. M., Hawkes, J. J., Spengler, J., Radel, S., Lawler, H., Devcic-Kuhar, B., Groschl, M., Coakley, W. T., and McLoughlin, A. J. (**2005**). "A new immobilization method to arrange particles in a gel matrix by ultrasound standing waves," Ultrasound Med. Biol. **31**, 261–272.
Gol'dberg, Z. (**1971**). "Radiation forces acting on a particle in a sound field," in *High Intensity Ultrasonic Fields*, edited by L. Rozenberg (Plenum Press, NY), pp. 109–117.
Gonzalez, R. C., and Woods, R. E. (**2008**). *Digital Image Processing* (Prentice Hall, Upper Saddle River, NJ), p. 58.
Gor'kov, L. (**1962**). "On the forces acting on a small particle in an acoustical filed in an ideal fluid," Sov. Phys. Dokl. **6**, 773–775.
Gould, R. K., and Coakley, W. T. (**1974**). "The effects of acoustic forces on small particles in suspension," in *Finite Amplitude Wave Effects in Fluids: Proceedings of the 1973 Symposium*, edited by L. Bjorno (IPC Science and Technology Press LTD, Guildford), pp. 252–257.
Griffith, C. K., Miller, C., Sainson, R. C., Calvert, J. W., Jeon, N. L., Hughes, C. C., and George, S. C. (**2005**). "Diffusion limits of an in vitro thick prevascularized tissue," Tissue Eng. **11**, 257–266.
Griffith, M., Jackson, W. B., Lagali, N., Merrett, K., Li, F., and Fagerholm, P. (**2009**). "Artificial corneas: A regenerative medicine approach," Eye **23**, 1985–1989.
Haralick, R. M. (**1979**). "Statistical and structural approaches to texture," Proc. IEEE **67**, 786–804.
Ino, K., Okochi, M., and Honda, H. (**2009**). "Application of magnetic force-based cell patterning for controlling cell-cell interactions in angiogenesis," Biotechnol. Bioeng. **102**, 882–890.
Jaklenec, A., Stamp, A., Deweerd, E., Sherwin, A., and Langer, R. (**2012**). "Progress in the tissue engineering and stem cell industry 'are we there yet?'," Tissue Eng. Part B Rev. **18**, 155–166.
Khademhosseini, A., Vacanti, J. P., and Langer, R. (**2009**). "Progress in tissue engineering," Sci. Am. **300**, 64–71.
Korff, T., and Augustin, H. G. (**1999**). "Tensional forces in fibrillar extracellular matrices control directional capillary sprouting," J. Cell. Sci. **112**(Pt 19), 3249–3258.
Larrivee, B., Freitas, C., Suchting, S., Brunet, I., and Eichmann, A. (**2009**). "Guidance of vascular development: Lessons from the nervous system," Circ. Res. **104**, 428–441.
L'Heureux, N., McAllister, T. N., and de la Fuente, L. M. (**2007**). "Tissue-engineered blood vessel for adult arterial revascularization," N. Engl. J. Med. **357**, 1451–1453.
Macchiarini, P., Jungebluth, P., Go, T., Asnaghi, M. A., Rees, L. E., Cogan, T. A., Dodson, A., Martorell, J., Bellini, S., Parnigotto, P. P., Dickinson, S. C., Hollander, A. P., Mantero, S., Conconi, M. T., and Birchall, M. A. (**2008**). "Clinical transplantation of a tissue-engineered airway," Lancet **372**, 2023–2030.
McAllister, T. N., Maruszewski, M., Garrido, S. A., Wystrychowski, W., Dusserre, N., Marini, A., Zagalski, K., Fiorillo, A., Avila, H., Manglano, X., Antonelli, J., Kocher, A., Zembala, M., Cierpka, L., de la Fuente, L. M., and L'Heureux, N. (**2009**). "Effectiveness of haemodialysis access with an autologous tissue-engineered vascular graft: A multicenter cohort study," Lancet **373**, 1440–1446.
Olausson, M., Patil, P. B., Kuna, V. K., Chougule, P., Hernandez, N., Methe, K., Kullberg-Lindh, C., Borg, H., Ejnell, H., and Sumitran-Holgersson, S. (**2012**). "Transplantation of an allogeneic vein bioengineered with autologous stem cells: A proof-of-concept study," Lancet **380**, 230–237.
Olson, J. L., Atala, A., and Yoo, J. J. (**2011**). "Tissue engineering: Current strategies and future directions," Chonnam Med. J. **47**, 1–13.
Pang, K. Y., Iznita, I. L., Fadzil, H. M. A., Hanung, A. N., Hermawan, N., and Vijanth, S. A. (**2009**). "Segmentation of retinal vasculature in color images," in *Innovative Technologies in Intelligent Systems and Industrial Applications* (IEEE, Malaysia), pp. 398–401.
Pijnappels, D. A., Schalij, M. J., Ramkisoensing, A. A., van Tuyn, J., de Vries, A. A., van der Laarse, A., Ypey, D. L., and Atsma, D. E. (**2008**). "Forced alignment of mesenchymal stem cells undergoing cardiomyogenic differentiation affects functional integration with cardiomyocyte cultures," Circ. Res. **103**, 167–176.
Priya, S. G., Jungvid, H., and Kumar, A. (**2008**). "Skin tissue engineering for tissue repair and regeneration," Tissue Eng. Part B Rev. **14**, 105–118.
Raghavan, S., Nelson, C. M., Baranski, J. D., Lim, E., and Chen, C. S. (**2010**). "Geometrically controlled endothelial tubulogenesis in micropatterned gels," Tissue Eng. Part A **16**, 2255–2263.
Raya-Rivera, A., Esquiliano, D. R., Yoo, J. J., Lopez-Bayghen, E., Soker, S., and Atala, A. (**2011**). "Tissue-engineered autologous urethras for patients who need reconstruction: An observational study," Lancet **377**, 1175–1182.
Saito, M., Daian, T., Hayashi, K., and Izumida, S. (**1998**). "Fabrication of a polymer composite with periodic structure by the use of ultrasonic waves," J. Appl. Phys. **83**, 3490–3494.
Shin'oka, T., Imai, Y., and Ikada, Y. (**2001**). "Transplantation of a tissue-engineered pulmonary artery," N. Engl. J. Med. **344**, 532–533.
Thery, M. (**2010**). "Micropatterning as a tool to decipher cell morphogenesis and functions," J. Cell Sci. **123**, 4201–4213.
Whitworth, G., and Coakley, W. (**1992**). "Particle column formation in a stationary ultrasonic field," J. Acoust. Soc. Am. **91**, 79–85.
Zheng, Y., Chen, J., Craven, M., Choi, N. W., Totorica, S., Diaz-Santana, A., Kermani, P., Hempstead, B., Fischbach-Teschl, C., Lopez, J. A., and Stroock, A. D. (**2012**). "In vitro microvessels for the study of angiogenesis and thrombosis," Proc. Natl. Acad. Sci. U.S.A. **109**, 9342–9347.